Jestr

Journal of Engineering Science and Technology Review 15 (3) (2022) 84 - 98

JOURNAL OF
Engineering Science and Technology Review

Research Article

www.jestr.org

Progress in High Performance in Oxychalcogenide Bicuseo: A Promising Thermoelectric Material for Energy Harvesting Applications

Shekhar D. Bhame* and Rishi Prasad

Symbiosis Institute of Technology (Deemed University) Lavale, Pune, 412115, Maharashtra, India

Received 28 October 2021; Accepted 6 July 2022

Abstract

BiCuSeO (BCSO) is one of the chalcogenides-based energy harvesting thermoelectric materials that have been studied since past one decade. BCSO based thermoeletrcic materials are attractive because of their inherent anisotropic properties as a result of their multi-layered structure which directly influences the thermoelectric figure of mertit ZT. This review primarily focuses on the evolution of BCSO based system up to the latest developments. First, we have discussed the various fundamental aspects of BCSO compounds followed by various strategies for tuning the thermoelectric parameters such as thermal conductivity and electrical conductivity. They have been discussed under various headings such as single carrier doping, co-doping technique, defect engineering, bandgap engineering, modulation doping and spin Seebeck effect. To summarize, this review compiles all the BCSO based compounds with high ZT as reported year wise.

Keywords: BiCuSeO, thermoelectric oxide, high *ZT* oxides

1. Introduction

Global energy demands have been increasing on a day-to-day basis. The depletion of fossil fuels has made the research community to think about alternative sources. Solar, hydrothermal, thermal and wind energy harvesting technologies have been known since decades. Thermoelectric energy harvesting is one such echo friendly energy harvesting technology that have been a topic of interest since 1930s. Though the principles governing thermoelectric power generation were earlier identified by Estonian physicist Thomas Johann Seebeck in the year 1822 [1], much interest in this field was gained after A.F Ioffe proposed the use of semiconducting materials for waste heat recovery applications in 1930s [2]. Materials like PbS, PbSe-PbTe, Bi_2Te_3-Sb_2Te_3 were the first few materials that received attention [3]. He also put forward the equation to measure the efficiency of thermoelectric materials and termed it as thermoelectric figure of merit "*ZT*".

$$ZT = \frac{S^2\sigma}{\kappa_e+\kappa_l}T \quad (1)$$

Where S (V/K) is the Seebeck coefficient, σ (S/m) is electrical conductivity, κ_e, and κ_l (W/m K) are the electronic and lattice contribution to thermal conductivity. Slack proposed that potential thermoelectric material should process electrical conductivity as exhibited by a metal and thermal conductivity as that of a glass. Such a material was classified as "Phonon Glass Electron Crystal (PGEC)" [4]. Obtaining such a crystal is particularly difficult because the electrical and thermal conductivity are related by Wiedemann-Franz law ($\kappa_e = LT\sigma$). Also, since Seebeck coefficient and carrier concentration are inversely related, when n increases, it leads to increase in electrical conductivity but decreases the S hence making it difficult to tailor the parameters for maximum efficiency.

However, various thermoelectric parameter has been optimised by Snyder *et al*. with respect to the carrier concentration. It was reported that maximum *ZT* and power factor for narrow bandgap semiconductors are when the carrier concentration is within the range of ~10^{19} – 10^{20} carriers/cm^3. Figure 1 shows the optimization of *ZT* by tuning the carrier concentration for Bi_2Te_3 [6]. The complex inter-relationships between the various thermoelectric parameters can be described based on the following equations:

$$S = \frac{8\pi K_B^2}{3eh^2}m^*T\left(\frac{\pi}{3n}\right)^{2/3} \quad (2)$$

$$\sigma = ne\mu = \frac{ne^2\tau}{m^*} \quad (3)$$

$$K_{tot} = \kappa_{lat} + \kappa_{ele} = \kappa_{lat} + L\sigma T \quad (4)$$

Where K_B is a Boltzmann constant, m^* is density of states effective mass, h is the Planks constant (6.6260×10^{-34} m^{2}kg/s), n being carrier concentration, e is charge of an electron (1.6021×10^{-19} coulombs), μ is carrier mobility, τ is relaxation time and K_{tot}, κ_{lat}, κ_{ele}, being total, lattice and electronic contribution to thermal conductivity and L is Lorentz number (2.44×10^{-8} W Ω K^{-2}) [7].

Although many state-of-the-art materials that belongs to different classes such as Skutterudites, Clathrates, Half Heusler's and Chalcogenides that are fairly efficient, high temperature heat recovery with these materials are a challenge. However, oxide-based materials possess high thermal stability, high melting point and hence could be used for high temperature applications. ZnO [8], In_2O_3 [9], $SrTiO_3$ [10], $Ca_3Co_4O_9$ [11], Na_xCoO_2 [12] and BiCuSeO [13] are a few oxides based system that have been widely studied to improve the thermoelectric parameters. In this review we would like to highlight the BiCuSeO based compound which

*E-mail address: shekhar.bhame@sitpune.edu.in
ISSN: 1791-2377
doi:10.25103/jestr.153.09

is an oxychalogenide based material that has been reported to exhibit high thermoelectric parameters than the rest of oxides. BiCuSeO was first recognised as potential thermoelectric material in 2010. The following graph (figure 2) depicts the growth of research interest on this class of materials since 2010.

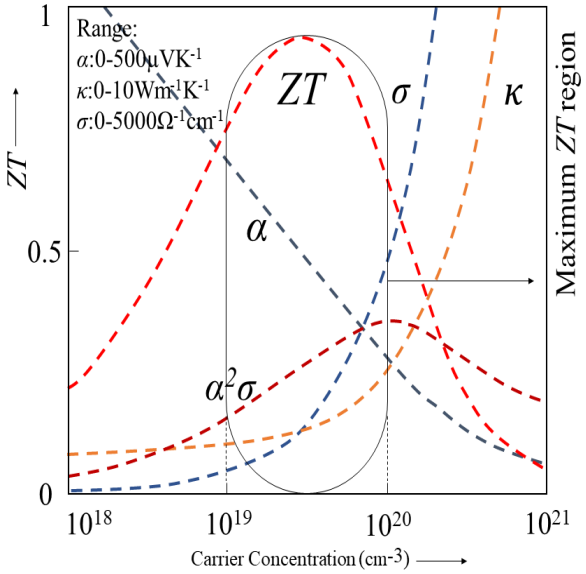

Fig. 1. Optimization of ZT by tuning the carrier concentration for Bi_2Te_3. Image adapted from Snyder et al [5] (Copyright © 1969, Nature Publishing Group.)

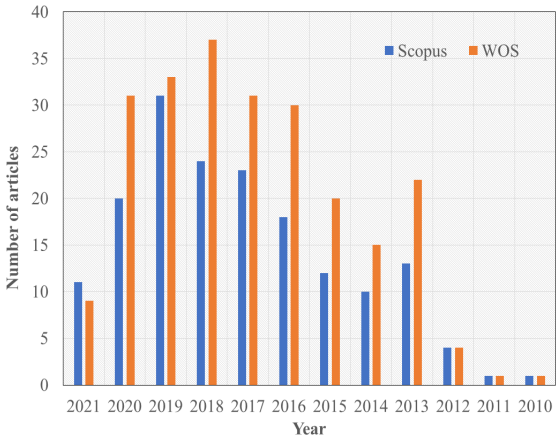

Fig. 2. The number of papers published since 2010.

BiCuSeO is an oxychalogenide based material that belongs to the tetragonal unit cell family with a space group of P4/mm. They exhibit a composite 2-D layered structure having alternatively stalked $(Cu_2Se_2)^{2-}$ and $(Bi_2O_2)^{2+}$ along the c axis of tetrahedral cell (figure 3). While $(Bi_2O_2)^{2-}$ layer acts as the charge reservoir insulating layer with ionic bonds, the $(Cu_2Se_2)^{2-}$ layer with covalent bond nature acts as conducting path for carrier transport.

The crystallographic, thermoelectric and elastic parameters associated with BCSO are as follows [14] [Table 1].

Computational studies show that BCSO has a multiband structure with indirect bandgap of 0.8 to 1 eV. The bottom of conduction band mainly consists of the Bi-6*p* states, while the top of the valence band consists of antibonding Cu 3*d*- Se 4*p* orbitals followed by nonbonding Cu-3*d* states (-1 to -3 eV). The bottom of the valence band consists of Bi-6*s* states that are -10 to -12 eV away from the valence band maximum. The valence band also consist of O2*p* states that are -5 to -7 eV away from the valence band maximum [15].

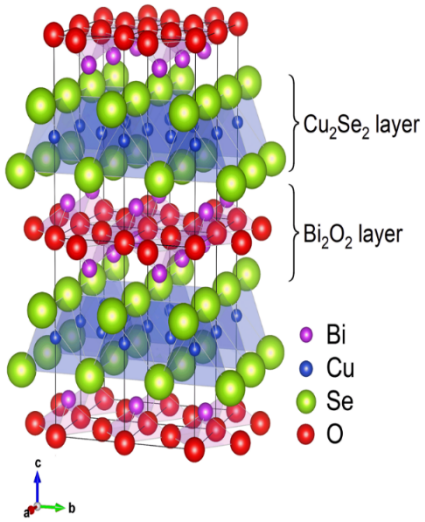

Fig. 3. Crystal structure of BiCuSeO simulated using VESTA.

Table1. Parameters associated with BiCuSeO.

Formula weight	367.4858
Crystal system	Tetragonal
Space group	P4/mm
Unit cell dimensions	a = 3.921 Å, α = 90° b = 3.921 Å, β = 90° c = 8.913Å, γ = 90°
Unit cell volume	137.06 $Å^3$
Z	2
Theoretical density	8.9 g cm^{-3}
Carriers concentration	$1x10^{18}$ cm^{-3}
Carriers mobility	22 $cm^2V^{-1}s^{-1}$
Band effective mass	Light hole band (0.18 m_e) Heavy hole band (1.1 m_e)
Seebeck coefficient	349 μVK^{-1}
Electrical conductivity	1.12 Scm^{-1}
Lattice thermal conductivity	0.55 $Wm^{-1}K^{-1}$
Longitudinal sound velocity	3290 ms^{-1}
Transverse sound velocity	1900 ms^{-1}
Average sound velocity	2107 ms^{-1}
Young's modulus	76.5 GPa
Debye temperature	243 K
Poisson ratio	0.25
Grüneisen parameter	1.5

In this review, we discuss about the evolution of BiCuSeO based oxychalogenides from the time of their identification as a potential thermoelectric material till the recent progress. The various strategies that have been followed to optimise the performance of BCSO such as, Single element doping, Dual

doping, Covalency tuning, Bandgap engineering, Spin Seebeck effect and Modulation doping which we would be discussing. We discuss promising materials under each sections in a chronological order.

3. Discussion

3.1. Strategies to enhance thermoelectric properties

3.1.1 Single element doping

Zhao *et al.* were the first group to identify BCSO based compounds to be promising thermoelectric material in 2010. They introduced Sr as the dopant which induces carriers in the reservoir layer and enhances electrical conductivity. Though BCSO is a *p*-type material with low electrical conductivity (470 S/m), Sr substitution ($Bi_{1-x}Sr_xCuSeO$) drastically increased the electrical conductivity to $4.8x10^4$ S/m at 293 K due to the semiconductive to metallic transition. BCSO exhibits high Seebeck Coeffienct due to its natural superlattice structure. Carriers confined within the superlattice usually leads to high Seebeck coefficient as seen in the case of artificial superlattice $SrTiO_3/SrTi_{0.8}Nb_{0.2}O3/SrTiO_3$. Although as percentage of Sr increases, the Seebeck coefficient (*S*) declines as high carrier concentration leads to low *S* (equation 2), the *S* value was still high such that the power factor of 580 $\mu Wm^{-1}K^{-2}$ at 873 K. While BCSO exhibited a *ZT* of 0.4 at 873 K, on Sr substitution at the Bi site resulted in a drastic increase in *ZT* upto 0.76 (x=0.075) as a result of high-power factor as thermal conductivity increases with Sr due to electronic contribution of thermal conductivity (0.6 $Wm^{-1}K^{-1}$ for the optimum concentration of x=0.075) [16]. Later, Barrateau *et al.* clarified that though electrical conductivity increased almost 100 times due to large carrier concentration power factor was still low due to decline in *S*. So, the overall high *ZT* was mainly due to low thermal conductivity as a result of intrinsic acoustic phonon scattering [15].

Though BCSO exhibit a low electrical conductivity, on substituting Ba in the Bi site, the negative charge induced in the $(Bi_2O_2)^{2+}$ insulating layer leads to carrier introduction into the conductive $(Cu_2Se_2)^{2-}$ layer thereby increasing the electrical conductivity from ~1.12 S/cm to ~535 S/cm for x= 0.15 at 300 K in $Bi_{1-x}Ba_xCuSeO$. While there was an improvement in the K_{tot} for pristine BCSO with temperature (0.54 at 300 K – 0.34 $Wm^{-1}K^{-1}$at 923 K , the K_{tot} for doped samples were more than the pristine BCSO (0.78 – 0.52 $Wm^{-1}K^{-1}$at 923 K). However, lattice thermal conductivity was less than the pristine BCSO which was attributed to point defects due to the strain field fluctuations or interatomic coupling force difference due to size difference (Ba~137.33 a.u and Bi~208.98 a.u) and mass difference (Ba^{2+}~1.34 Aº and Bi^{3+}~0.96Aº). Though K_{tot} increase with carrier concentration (i.e Ba doping), it is still lower enough to give rise to promising *ZT* of 1.1 at 923K for x=0.125 in $Bi_{1-x}Ba_xCuSeO$ [17].

$Bi_{1-x}Ca_xCuSeO$ with varying Ca concentration showed a promising improvement in the electrical conductivity from 2.13 S/cm (x=0) to 509 S/cm (x=0.125) as the charge carrier concentration increased with Ca concentration. As expected, the Seebeck coefficient decreased after x=0.075 and still managed to show a power factor greater than 500 $\mu W/mK^2$. The large Seebeck coefficient is suspected to be because of the large effective mass. Point defects and reduced grain size further lead to a reduced κ_{lat} from 0.78 to 0.5 $Wm^{-1}K^{-1}$at 425 K with increase in Ca percentage. These factors lead to a low thermal conductivity of <0.8 $Wm^{-1}K^{-1}$ for all the samples at 773 K leading to *ZT* of 0.8 at 773 K for x=0.075 [18]. x=0.10 exhibited an electrical conductivity of 270 S/cm at 300 K as compared to 1.12 S/cm for BCSO. This increase in electrical conductivity was due to the holes that are induced in $(Cu_2Se_2)^{2-}$ layers as a result of the substitution of Bi with Ca in $(Bi_2O_2)^{2+}$ leading to hole transfer from layer $(Bi_2O_2)^{2+}$ to $(Cu_2Se_2)^{2-}$. The mechanism behind this transfer is as follows:

$$2(Bi_{1-x}Ca_xCuSeO) = (Bi_{2-2x}Ca_{2x}O_2)^{(2-2x)+}+(Cu_2Se_2)^{2-}+2xh^+$$

Here, h^+ is the holes crated by the substitution of Bi^{3+} with Ca^{2+}. As seen already, Ca doping leads to decrease in thermopower to 198 µV/k at 923 K from 120 µV/k at 300 K for x=0.10 which is less as compared to the pristine BSCO. Though the K_{tot} increased with Ca concentration, still is less than 0.55 $Wm^{-1}K^{-1}$ at 923 K. However, K_{tot} exhibited considerable reduction on Ca doping as a consequence of point defect scattering leading to a reduction from 0.88 $m^{-1}K^{-1}$ (undoped) to 0.75 $Wm^{-1}K^{-1}$ (x=0.10) at 300 K. Point defects were due to the strain field fluctuations or interatomic coupling force difference due to size difference and mass difference between the dopant and host lattice. Results revealed that the low thermal conductivity in these compounds is because of high gruneisan parameter as high gp is due to high degree of bond anharmonicity due to Bi^{3+} and low young's modulus as lower young's modulus leads to weaker bonds or 'soft bonding' slowing down the phonons. These parameters leads to a *ZT* of 0.9 at 923 K for x=0.10 [19].

Though Pb doped BCSO were studied earlier by Pan *et al.*, they identified the solubility limit close to x=0.06 [20]. While they identified maximum power factor (5.25 $\mu Wcm^{-1}K^{-2}$) for x=0.03, Liu *et al*. obtained a power factor close to 5.6 $\mu Wcm^{-1}K^{-2}$ for x=0.08. *ZT* was not reported by Pan *et al*., Liu *et al.* obtained a *ZT* of 0.95 at 873K for x=0.08. The improvised electrical conductivity as a result of increase in carrier concertation due to Pb doping and low thermal conductivity were responsible for this improvement [21]. Followed by this work, Lan *et al.* carried out the same composition and were able to obtain a very high *ZT* of 1.14 at 893K. This spike in *ZT* was mainly because of large variation in power factor. While Liu *et al*. reported a PF of 5.6 $\mu Wcm^{-1}K^{-2}$, they could obtain a large PF of 7.3 $\mu Wcm^{-1}K^{-2}$ along with reduced κ_{lat} of 0.4-0.6 $Wm^{-1}K^{-1}$ at 823K due to the scattering of phonons by nanodot formations seen from SEM and TEM images in figure 4 [22].

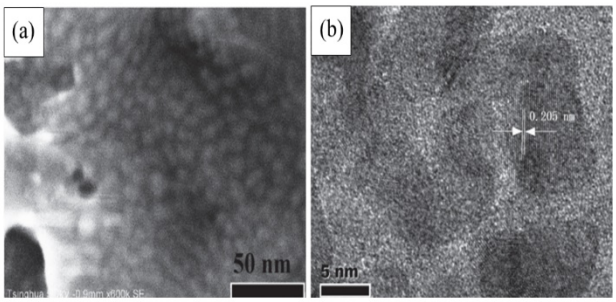

Fig. 4. The higher SEM image for 6% Pb doped BCSO exhibiting nanodots (a) and TEM image of the fussy boundaries and nanodots (b).

Meanwhile Sui *et al.* identified the effect of texturization on Ba doped samples. Making use of the inherit anisotropy property, hot-forging technique enabled them to push *ZT* upto 1.4 at 923 K for 12.5% Ba doping ($Bi_{1-x}Ba_xCuSeO$, x=0.125)

for three times hot forged sample. Since hall effect measurements showed not so promising carrier concentration improvements, the hike in electrical conductivity from 450 to 700 S/cm at room temperature was attributed to improvement in carrier mobility. This improvement leads to increase in PF (from 6.3-8.1 $\mu Wcm^{-1}K^{-2}$ at 923 K) and double fold increase (2-4 $cm^{-2}V^{-1}s^{-1}$for non-textured and 3 times hot-forged sample) in carrier mobility. Such an improvement was possible due to higher degree of grain alignment induced by hotforging technique. Grain alignment was seen to increase with number of hot forging steps. The inverse pole figures shown in figure 5 shows clearly that the texturization was maximum for the most hot forged sample and the orientation was along (001) direction. Since the density of grain boundary decrease along the aligned direction, both electrical and thermal conductivity increases. Measurement along parallel direction exhibited a decline in thermoelectric parameters as the number of grain boundaries are more along this direction. Seebeck coefficient was seen to be unaffected by texturization to exhibit ~187 μV/K at 923 K for all samples. Though thermal conductivity increased with hot forging, high electrical conductivity and power factor for the hot forged sample gave rise to a *ZT* of ~1.4 at 923 K [23].

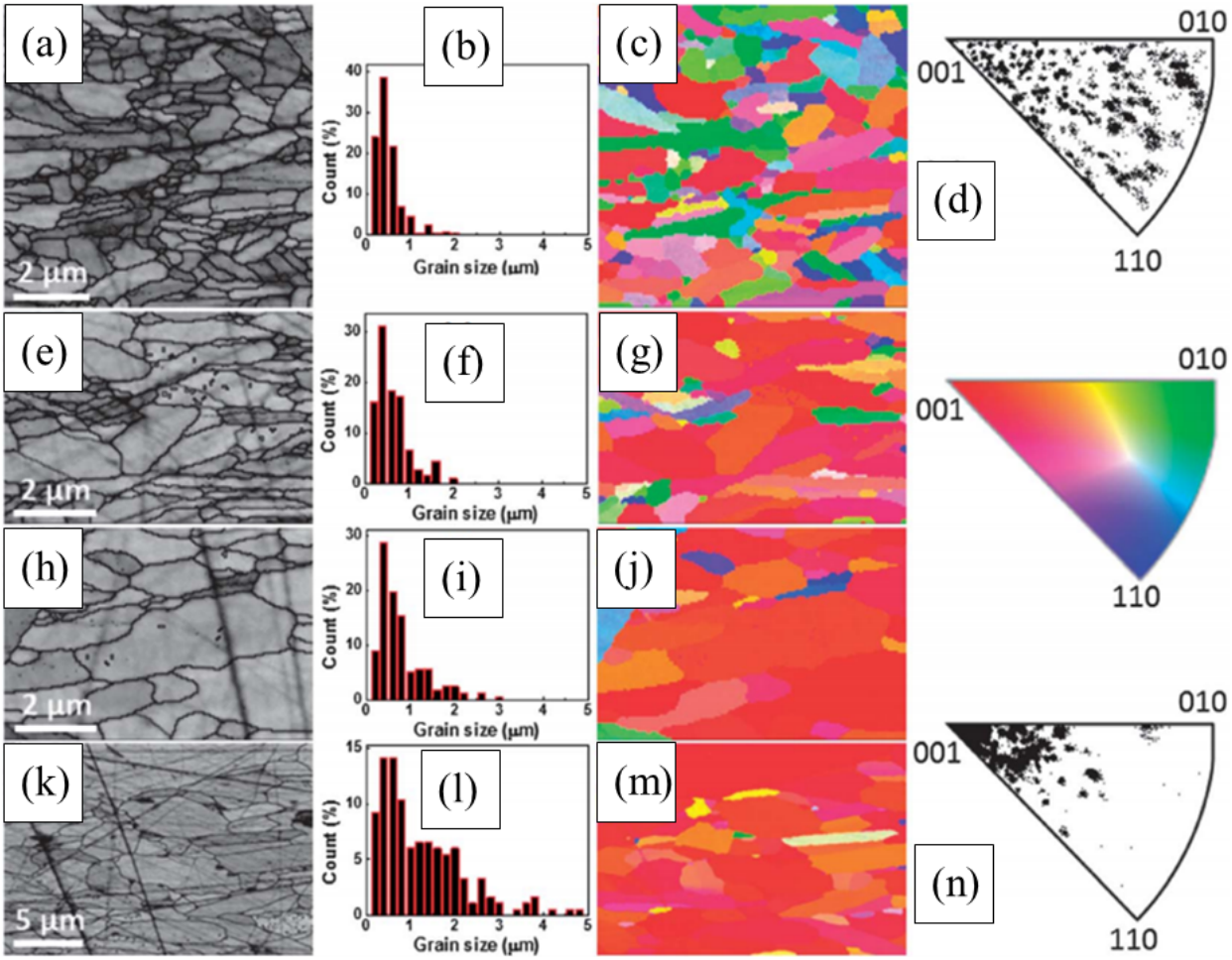

Fig. 5. The microstructure (a, e, h, k), grain size distribution (b, f, i, l), z-Euler images (c, g, j, m) of 0, 1, 2 and 3 T⊥ samples respectively and the inverse pole figures (d, n) for 0 and 3T⊥ samples.

Understanding the limitations of other dopants such as Ba, Mg, Pb, Ca and Sr, Li *et al.* carried out Na doping in the BCSO matrix. They suggested that, since a single alkali metal atom can donate two holes and their ionic radius is close to alkaline-earth metals, it can act as a better dopant. Na doped BCSO exhibited higher carrier concentration than the rest of the studied materials (Ba, Mg, Pb, Ca and Sr). The electrical conductivity improved to 125 S/cm for x=0.015 at 300 K. This composition exhibits the highest power factor of 8.0 $\mu Wcm^{-1}K^{-2}$ at room temperature. The huge mass fluctuation between the Na and Bi atoms lead to a reduction in $\kappa_{lat}$with increasing concentration and leading to K_{tot} of 0.5 $Wm^{-1}K^{-1}$ at 923K. This is mainly attributed to point defects created by the Na atoms. These factors lead to a *ZT* of 0.91 at 923 K for x=0.015 in $Bi_{1-x}Na_xCuSeO$ [24].

Although attempts were made to partially substitute Cu, their *ZT* never crossed 0.8 until Ren *et al.* reported their work. They reported a *ZT* of 0.90 at 873 K for 1% substitution of Zn at Cu site. This improvement was mainly because of the enhancement in electrical conductivity due to promising mobility (0.812 $cm^2V^{-1}s^{-1}$) and carrier concentration ($1.50x10^{20}$ cm^{-3}) along with power factor due to Zn substitution. While electrical conductivity improved from ~3000 to 5000 S/m, power factor improvised from ~3 to 4 $\mu Wcm^{-1}K^{-2}$ at 873K [25].

In an attempt to optimise methods for better TE performance in BCSO based compounds, out of SSR and SHS, it was seen that SHS could outperform SSR method. Electrical conductivity (10 to 44 S/cm at 800 K for SSR and SHS respectively) and power factor (1.5 to 3.6 $\mu Wcm^{-1}K^{-2}$ at 800K for SSR and SHS respectively) increased drastically. An increase in grain size as well as grain alignment were seen to be the cause for this improvement. It was also seen that the K_{tot} was also considerably lesser than the SSR sample. Since the study proved SHS to be promising, this method was followed for preparing pure and Pb doped BCSO samples.

The study suggested that, 4% Pb incorporation could enhance the *ZT* from ~0.45 to upto 0.91 at 873 K. This increment was mainly due to the increase in electrical conductivity and reduction in thermal conductivity as a result of introduction of nano pores that are equally distributed and refined grains along with point defects. However, the increment in power factor was mainly attributed to reduction in bandgap and increase in effective mass with doping concentration [26]. Although a *ZT* of 0.91 was reported for Na (1.5%), higher doping was not carried out. Zhang *et al.* carried out the synthesis by doping concentration close to the solubility limit of Na (8%). Although electrical conductivity, Seebeck Coeffienct and power factor were very close to the results obtained by Li *et al.*, they could obtain a very low κ_{lat} <0.4 $Wm^{-1}K^{-1}$ while κ_{lat} reported by Li *et al.* was ~0.42 $Wm^{-1}K^{-1}$. This reduction in $\kappa_{lat}$was mainly due to the presence of point defects, secondary phases and precipitates of nanoscale Na_2CO_3 and Na_2SeO_3 particles. This led to an enhancement in *ZT* to 0.97 at 873 K [27].

For the first time, Farooq *et al.* reported Cd doping at the Bi site. Since Cd is a lighter atom than Bi, replacing Bi partially would bring in a week coulomb force among the layers which could slow down the phonons. At a higher Cd doping concentration, the electrical conductivity increased as the carrier concentration increases. 5% doping of Cd resulted in 73 S/cm which is 110% higher than what was reported for pristine BCSO at 923 K. Almost 50% suppression in lattice thermal conductivity (~0.29 $Wm^{-1}K^{-1}$) due to the small grains and increase in grain boundaries and improvement in power factor (450 $\mu W/m.K^2$ at 923 K) was seen on Cd doping. The combined effect of all resulted in a *ZT* of 0.98 at 923K [28].
Yang *et al.* in 2016, obtained a *ZT* of ~1.2 at 923 K for x=0.06 in $Bi_{1-x}Cu_xSeO$. An increase in carrier concentration with doping resulted in increasing electrical conductivity and reduction in Seebeck coefficient. Though Pb doping did not decrease the lattice thermal conductivity, the increment in power factor lead to a *ZT* of 1.2 at 923 K for the 6% doped sample [29].

Zhu *et al*. in 2016 reported the effect of pressured sintering on thermoelectric parameters. Interestingly, the pressure sintered samples reported to exhibit a large change in *ZT* as compared to the pressureless sintered sample. Though the electrical conductivity of pressure sintered sample was more than the other, very high Seebeck coefficient exhibited by the pressure sintered sample resulted in a high power factor (2.1 $\mu W/cm.K^2$). In addition to these results, the fine grains and large number of grain boundaries lead to a marginal decrease (almost half) in thermal conductivity (0.56 $Wm^{-1}K^{-1}$ for pressureless sintered and 0.42$Wm^{-1}K^{-1}$ for the pressure sintered sample) and exhibited a *ZT* of 0.4 at 800 K [30].

However, a potential of replacing Se site completely with Te atoms exhibited a huge improvement in electrical conductivity mainly due to the least (0.4 to 0.5 eV) bandgap as compared to the S (1.1 eV) and Se (0.8 eV) samples. Though first principle calculations and neutron diffraction data suggest that low thermal conductivity of such compounds are due to the low- energy vibrational modes of Cu. It was observed that as the atomic radii increased, thermal conductivity deteriorated. Te doped compound gave rise to a further reduction in thermal conductivity (0.39 $Wm^{-1}K^{-1}$ at 650 K) due to the weak bonding between Cu and Te atoms leading to slower sound velocity and strong optical-acoustic scattering as seen in the figure (which otherwise contribute to increase in thermal conductivity). These effects lead to an improvement of *ZT* from 0.3 (BCSO) to 0.65 (BCTO) at 650 K [31]. Though replacing Cu site with Ag has been reported with improvement in *ZT*, *ZT* of more than 1 has not been reported yet [32, 33].

While trying to understand the effect of Sn doping at the Bi site by a unique two step solid state synthesis by Das *et al.*, a promising *ZT* of 1.09 was obtained for the sample with no dopants. While the secondary phase formation (SnO_2) lead to increase in electrical resistivity and thermal conductivity, pristine sample outperformed the doped samples. However, it has been highlighted that, the intention of doping Sn was to increase the hole concentration provided if it stays in the +2-oxidation state. But XPS results revealed Sn to be in +4 state hence reducing the hole concentration thereby increasing the resistivity. The Bi and O vacancies created for the pristine sample lead to increase in carrier concentration leading to metallic character. These vacancy effects along with all length scale scatting mechanisms seen in the microstructure and mass fluctuation scattering due to high atomic radii Bi atom lead to relatively the lowest lattice thermal conductivity of 0.19 W/m-K and an electrical conductivity of 0.025 mΩ-m at 773 K leading to an overall *ZT* of 1.09 [34].

A study by Ren *et al.* showed that unlike the previous reports, they could obtain three PF maxima on doping Pb. They studied the variation of thermoelectric parameters with respect to doping. Results show that at a lower concentration of the dopants, the fermi level shifted close to the valence band thereby leading to an increase in carrier concentration. Thus, the DOS effective mass was tuned as the fermi level came close to the valence band leading to the first peak PF.
On further addition of dopants, second peak PF was seen as a consequence of the fermi level lying inside the valence band whereby the electrical conductivity and Seebeck coefficient was tuned leading to second PF peak (figure 6). It has to be noted that as the % of Pb increases, carrier mobility declined. Though the carrier mobility reported are higher than the pristine sample, the net change is downwards. Involvement of heavy band in the electrical conduction and ionized impurity scattering were held responsible for this. While the pristine sample followed a $T^{-1.5}$ relation, on doping it gradually changed to $T^{-0.5}$ which is a characteristic of ionized impurity scattering. And on compositing the base matrix with Pb, i.e. at higher addition of more than 12%, the PbSe and CuSe nanoprecipitate formation lead to the third peak PF (figure 6). Such an improvement was mainly due to the carrier mobility induced by PbSe. One of the key highlights of this study was to show how by just getting the fermi level close to the first DOS peak we can attain a high PF without following other techniques such as texturing, modulation doping etc. Along with these effects, the lattice thermal conductivity was reported to be lower than the pristine sample due to all scale hierarchical scattering process such point defect scattering, mesoscale grain boundary scattering and scattering due to the formation of nanostructures in the matrix. These structural features lead to an ultra low lattice thermal conductivity of as low as ~0.13 W $m^{-1}K^{-1}$ at 873K (2% Pb doped) well below the Cahills glassy limit of ~0.59 W $m^{-1}K^{-1}$. These features lead to high ZT of 0.9 , 1.1 and 1.3 at 873K at various doping levels as shown in the figure 6b [35].

A unique strategy was followed by Feng *et al.* where a two-level optimisation technique to tune the thermoelectric properties was followed. Firstly, doping Bi site with In was done to increase the carrier mobility as a consequence of the widening of bandgap which enhances the electrical transport properties followed by grain refinement. Indium doping essentially leads to an increase in influence of light bands which has a crucial role in mobility enhancement (figure 6).

Hence electrical conductivity enhancement was seen from ~25 to 100 S/cm with doping.

It was seen that, Seebeck effect had a negative impact on doping In. This might be due to the decrease in effective mass of In as compared to Bi. However, a huge enhancement in PF was seen from ~0.28 $mWm^{-1}K^{-2}$ to 0.4 $mWm^{-1}K^{-2}$, thanks to the electrical conductivity enhancement. Although, it was seen that the thermal conductivity decreased with temperature, thermal conductivity reported for doped samples were higher than the pristine sample . BCSO is known for its low thermal conductivity mainly because of the presence of Bi, which is a heavy element. Now, on replacing/doping with In (a lighter element) essentially reduces the Bi% leading to higher thermal conductivity. However, In doping alone enhanced the net ZT from ~0.55 to ~0.61 (for 6% In doped sample) at 873K. In the second part of optimisation, varying percentage of fine and coarse powder were milled together. An optimum ratio of fine to coarse powder mixture of 80%, i.e. 80% fine powder 20% coarse gave rise to a huge enhancement in the electrical conductivity leading to similar enhancement in PF. This coupled with low thermal conductivity enabled the mixture of 80% fine powder to reach a high ZT of 1.08 at 873K. While the increase in electrical conductivity was attributed to increase in the carrier concentration as a consequence of formation of Cu vacancies. Decrease in thermal conductivity was attributed to the phonon scattering due to grain refinement with increase in fine powder [36].

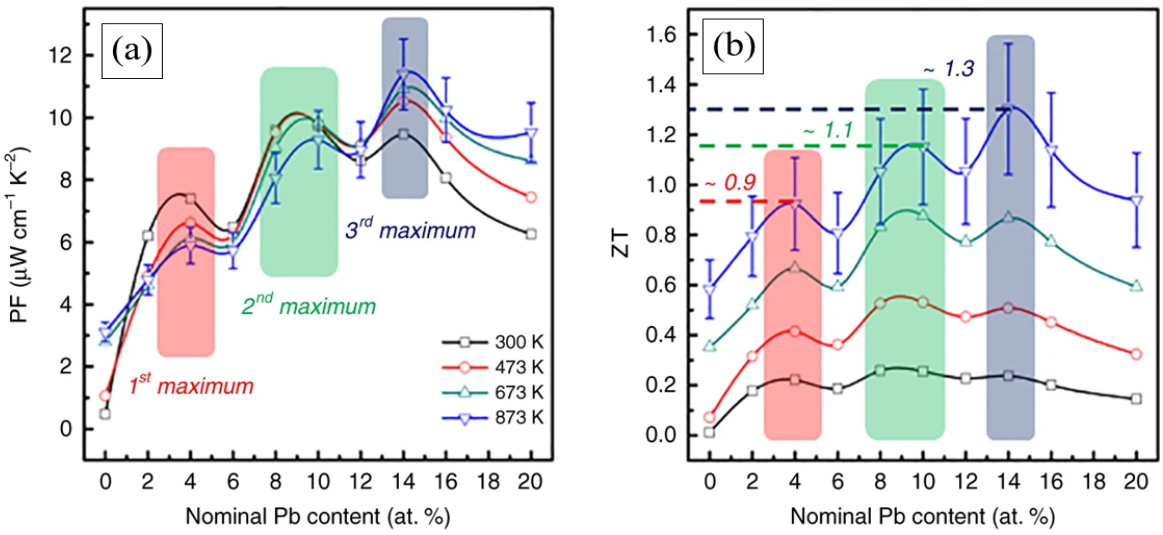

Fig. 6. Variation of power factor and ZT with respect to % of Pb in BCSO.

Lately, Feng et al reported a single element (Y) doped BSCO exhibited improved thermoelectric figure of merit. The 6 to 8% doped sample at Bi site exhibited excellent improvement in the electrical conductivity. Incorporation of Y enhanced the carrier concentration leading to such a change. This can also be understood based on the equation. It was seen as; 8% doped sample exhibited a Seebeck coefficient less than the pristine sample for the same reason.

3.1.2 Co-doping approach:

On looking at the previous works, it was seen that single element doping has led to the improvement in either electrical conductivity or thermal conductivity but simultaneous improvement in both was only moderate. In order to combine both the effects, i.e., reduction in thermal conductivity and increase in electrical conductivity, Liu *et al.* carried out dual doping technique whereby, Pb acted as agent for the improvement in electrical conductivity whereas Ca played the role to reduce thermal conductivity. Since Pb has a delocalised 6*s* orbital that has a lone pair of electrons and due to an increased effective mass, Seebeck coefficient and electrical conductivity improves better than any other elemental doping. On the other hand, Ca induces both mass fluctuation (difference in mass), size and strain field fluctuation (difference in interatomic coupling force) leading to minimum thermal conductivity. Though the solubility limit of Pb is 6 to 7%, higher amount of Pb exhibited formation of nanoprecipitates which lead to reduction in lattice thermal conductivity. Though the pristine BCSO are known to exhibit high Seebeck coefficient, upon dual doping, it decreases to 175 μV/K at 873 K which 3 times is lower. Thus, the improvement in electrical conductivity coupled with a moderate Seebeck coefficient gives rise to a promising power factor of $1.0x10^{-3}$ $Wm^{-1}K^{-2}$ for x=0.06 as compared to $2.2x10^{-4}$ $Wm^{-1}K^{-2}$ at 873K. The formation of Bi rich nanoinclusions and CaO_2 contributes to phonon scattering leading to a reduction in lattice thermal conductivity from ~3.8 to ~2.9 $Wm^{-1}K^{-1}$ at 873K. All the factors combined together lead to a high *ZT* of ~1.5 at 873 K. A comparison of this composition (x=0.06) with the singly doped composition (Ca or Pb) are given in the figure 7. It can be seen that codoped composition out performs the singly doped compositions in terms of electrical conductivity (figure 7a) and power factor (figure 7c) in particular. Better power factor and reduced thermal conductivity (figure 7e) further leads to improvement in ZT (figure 7f) in the whole temperature range as compared to the individually doped compositions [37].

It was already known that since Pb has a delocalised 6*s* orbital that has a lone pair of electrons and due to an increased effective mass, Seebeck coefficient and electrical conductivity improves better than any other elemental doping in the BCSO system as reported by Liu *et al.* [37]. Te was identified earlier as an attractive dopant at the Cu site to decrease the thermal conductivity. A co-doping of both these materials. i.e Pb at Bi site and Te at the Se site was explored by Ren *et al.* They observed that though carrier concentration

decreased drastically on Te doping, presence of Pb helped in retaining the high electrical conductivity, Seebeck Coeffienct and power factor. Though the carrier concentration decreased with Te doping, the carrier mobility increased. This increase in carrier mobility was attributed to the decrease in effective mass on doping Te in the BCSO system. Self-propagating high temperature method lead to the formation of all scale hierarchical structures such as nanoinclusions, point defects, grain boundaries etc leading to further reduction in thermal conductivity to amorphous limit. This combination also reported to exhibit weak carrier scattering. Although the electrical conductivity slightly declined on Te co-doping as compared to only Pb doped BCSO, Seebeck coefficient and power factor were higher for the co doped samples. The improvement in Seebeck Coeffienct was clearly due to the decrease in carrier concentration as discussed before which lead to a higher power factor of ~6 μW/cm.K^2 near 873 K. Further on comparing with computational data by Debye Callaway model, the SHS yielded rich in microstructural features enabling scattering of phonons due to point defects created by Te atoms as they have higher ionic radii as seen in figure 8.

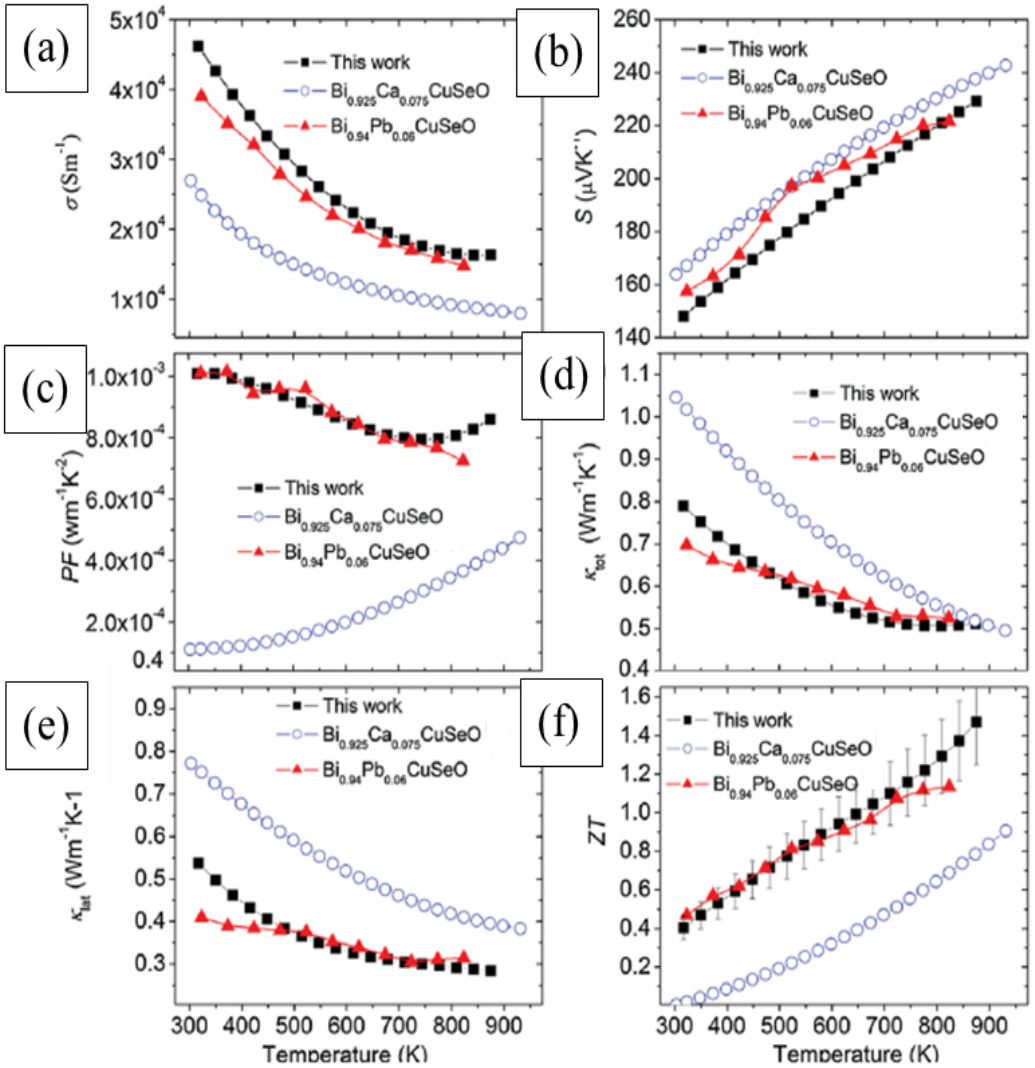

Fig. 7. Comparison of (a) the electrical conductivity, (b) the Seebeck coefficient, (c) power factor, (d) total thermal conductivity, (e) lattice thermal conductivity, and (f) the figure of merit ZT , respectively) of $Bi_{0.88}Ca_{0.06}Pb_{0.06}CuSeO$ with respect to singly doped compositions.

Along with these defects they also reported nanodot formation (figure 9a) of Cu_2Se_x (identified with interplanar spacing of 2.080 Å and 3.320 Å corresponding to (541) and (211) crystal faces Figure 8b), Pb, Te and Se and secondary phase corresponding to $Cu_7Te_{4-x}Se_x$ (as seen from the HRTEM images shown in figure 8d) formation of grain boundaries (figure 8c) along with the collapsed phase of Cu_7Te_4 (identified with the interplanar distance of d=4.066Å) which again contributes to decrease in thermal conductivity. These factors lead to a huge improvement in *ZT* from 0.5 to 1.2 at 800 K [38]. In a report by Sun *et al.* the same two step solid state synthesis was followed to synthesise Mg and Pb codoped BCSO. However, a much lower heating and hopressing time was followed as compared to the report by Das *et al.* [34]. An improved electrical conductivity was seen as the doping increased which was attributed to the increase in carrier concentration as shown in figure 9.

Also, it was seen that there was a linear relationship between the electrical conductivity and $T^{1.5}$ (insert figure 9) indicating that acoustic phonon scattering being the cause for metallic behaviour also that the impurity is degenerately doped aver the whole temperature range. While the carrier concentration increase, it is known that Seebeck coefficient ideally decreases. This was clear from the Seebeck Coeffienct data. Since there the difference between electrical conductivity and Seebeck Coeffienct was large for the pristine and doped samples, power factor reported was 2.3 μW/cm-K^2 and ~8.5 to 10.5 μW/cm-K^2 respectively at 750K. Though

thermal conductivity increased on doping (0.79 $Wm^{-1}K^{-1}$ at 750 K for x=0.09), relatively the reported thermal conductivity was lower than that of the other oxide-based materials. This leads to almost 2.1 times higher (upto 1.19 at 750 K) *ZT* for the doped samples as compared to the pristine (0.4 at 750K) [39].

Previous reports suggest that co-doping is an effective technique to tune the thermoelectric parameters. Feng *et al*. in 2018 reported the influence of Ba and Pb co-doping in BCSO matrix ($Bi_{1-x-y}Ba_xPb_y$ CuSeO). They observed that the carrier concentration increased with concentration of dopant (1.21 to $94.13x10^{19}/cm^3$ for pristine and doped sample i.e. x=y=0.06 respectively) leading to higher electrical conductivity than the pristine material. Such an improvement can be understood from the following mechanism:

$$2(Bi_{(1-x-y)}\ Ba_y\ Pb_x\ CuSeO) = (Bi_{(2-2x-2y)}Ba_{2y}Pb_{2x}O_2\ )^{(2-2x-2y)+} + (Cu_2Se_2)^{2-} + 2(x+y)\ h^+$$

i.e. carriers are induced into the conductive layer $(Cu_2Se_2)^{2-}$ transferred from insulating layer $(Bi_2O_2)^{2+}$ by the substituting Bi^{3+} with Ba^{2+}/Pb^{2+} atoms. Since high carrier concentration leads to low Seebeck coefficient as per the equation 2, Seebeck coefficient was seen to decrease as the percentage of dopant increased. The power factor was reported to be 0.66 $mWm^{-1}K^{-2}$ for x=y=0.06 while it was 0.28 $mWm^{-1}K^{-2}$ for the pristine sample. Though the thermal conductivity measured for pristine sample were small, the doped samples exhibited increase in thermal conductivity with doping. The replacement of comparatively lighter atoms such as Ba and Pb with Bi resulted in high sound velocity. The Bi-O bond is weaker than Ba/Pb-O leading to high frequency lattice vibrations, weak acoustic scattering and high thermal conductivity. However, at high doping concentration there was a slight change in this trend probably due to the formation of Ba/Pb nanoinclusions that scatters the phonon. A *ZT* of 1.01 which was 2.36 times higher than the pristine sample was thus observed for x=y=0.06 at 873 K [40].

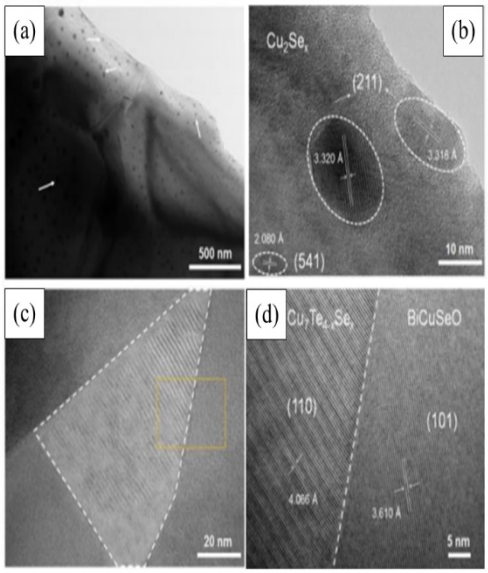

Fig. 8. TEM image showing homogeneously distributed nanodots in $Bi_{0.96}Pb_{0.04}CuSeO$, white arrows show that they spread both near the surfaces and in the interior of grains, (b) the lattice fringe measurement of nanodots through high resolution transmission electron microscope (HRTEM) (c) TEM image of nanoscale inclusions ($Cu_7Te_{4-x}Se_x$) in $Bi_{0.96}Pb_{0.04}CuSe_{0.95}Te_{0.05}O$, HRTEM image for dotted yellow-square-area in (c)

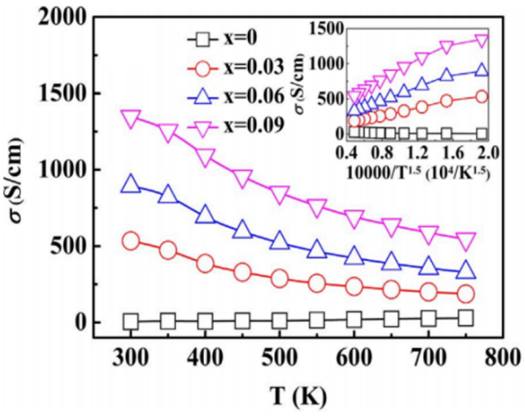

Fig. 9. Temperature dependence of electrical transport properties of $Bi_{1-2x}Mg_xPb_xCuSeO$ (plot of σ versus 10,000/T1.5 in the inset).

On an attempt to understand the effect of synthesis process on the thermoelectric parameters, the same team reported that, out of annealing and mechanical alloying, mechanical alloying lead to a higher carrier concentration that naturally lead to improved electrical conductivity. It was also seen that mechanical alloying lead to ~83% improvement in power factor and thermal conductivity followed by ~73% improvement in the *ZT* value. This optimization of technique was first done on pristine BCSO. After identifying the right synthesis process (mechanical alloying), Ca/Pb doped BCSO was synthesised by the same route. It was seen that for higher dopant concentration, i.e for x=0.06 and 0.08 in $Bi_{1-2x}Ca_xPb_xCuSeO$ exhibited higher electrical conductivity which was attributed to increase in hole concentration with doping. Though the thermal conductivity also increased with doping, due to high power factor, the highest *ZT* reported for x=0.08 was 1.15 at 873 K [41].

It was known already from the previous studies that Pb doping at the Bi site can leave a remarkable effect on the electrical properties. It was also proven that Ag substitution can reduce lattice thermal conductivity while the electrical conductivity enhancements were reported to be very little [42]. Li *et al.* co-doped Pb and Ag in the Bi and Cu site respectively thereby targeting to enhance the electrical conductivity and reduction in lattice thermal conductivity. Electrical conductivity increased from 40 S/cm to ~166 S/cm for x=0.06 at 864K. The electrical conductivity enhancements in the codoped samples were not found to be due to Ag incorporation but Pb alone. Hall data showed a drastic improvement in the carrier concentration (figure) with doping. The carrier mobility was however found to be low as a result of acoustic phonon scattering which is a characteristic of BCSO based compounds. Although the role of Ag can't be completely ignored as from the literature it is seen that Ag enhances carrier mobility, the carrier mobility reported in this case is higher than single doped Pb. The moderate Seebeck coefficient of ~190 μV/K coupled with high electrical conductivity enabled a very high PF of greater than 600 $\mu Wm^{-1}K^{-2}$ at 864K while the undoped exhibited a PF only near 300 $\mu Wm^{-1}K^{-2}$. It is to be noted that, the Seebeck coefficient reported for all the doped samples were less than the pristine sample since the effective mass was reduced for the codoped samples. Thermal conductivity studies showed a lower conductivity for the codoped samples than the single doped (Pb) doped one. A thermal conductivity of 0.6 W/mK was reported for the codoped sample while 1.3W/mK was for the singly doped sample. This reduction was mainly attributed to the reduction in lattice thermal conductivity enhancement

as a consequence of point defects created due to mass and radius fluctuations between Ag and Cu in BSCO (Ag ≈ 108 g/mol, Cu ≈ 64 g/mol; Ag^{+} ≈ 1.26 Å, Cu^{+} ≈ 0.96 Å). It has to be also noted that though thermal conductivity was lesser than the Pb doped sample, it is still higher than Ag doped sample as the grain size grew with Pb doping. However, an improved ZT was reported to be 0.95 for x=y=0.06 at 873K [43].

4. Defect Engineering

Copper deficiencies were created in the conductive $(Cu_2Se_2)^2$ layer by Liu *et al.* that resulted in a large increase in electrical conductivity. The electrical conductivity increased from 470S/m to 5.3x10^3 S/m at 923 K for pristine BCSO and $BiCu_{1-x}SeO$ (x=0.975) respectively as there was an increase in hole carriers created because of Cu deficiencies in the $(Cu_2Se_2)^2$ layer. Though Seebeck coefficient decreased (from 353 µV/K to ~250 µV/K) with the introduction of Cu deficiencies due to large hole concentration, the power factor was maximum for x=0.975 at 923 K. These effects coupled with a low thermal conductivity of 0.5 $Wm^{-1}K^{-1}$ lead to an improved *ZT* of 0.81 at 923 K [44].

Introducing Cu vacancies have been studied earlier and have proved to be a route to enhance the *ZT* of BCSO. Li et al studied the effect of creating dual vacancies. i.e. vacancies due to both Bi and Cu. Although the electrical conductivity increased for Bi0.975Cu0.975SeO from 1300 to 4700 S/m, it was still less than the conductivity by $BiCu_{1-x}SeO$ (x=0.975) synthesised by Liu *et al.* [44]. Seebeck coefficient decreased from ~380 to 300 µV/K at 750 K for pristine and vacancy created sample. However, it is to be noted that, $BiCu_{1-x}SeO$ (x=0.975) showed a Seebeck coefficient of ~225 µV/K which was much lower leading to a lower power factor. However, the thermal conductivity was much lower (0.37 $Wm^{-1}K^{-1}$ at 750 K) than the $BiCu_{1-x}SeO$ leading to an enhanced *ZT* of 0.84 at 750 K. The reduction in thermal conductivity was however attributed to the all-length scale phonon scattering. i.e. long wavelength scattering by grain boundaries, medium wavelength phonon scattering by supper lattice structure and the short wavelength scattering by the Bi/Cu vacancies as shown in figure 10 [45].

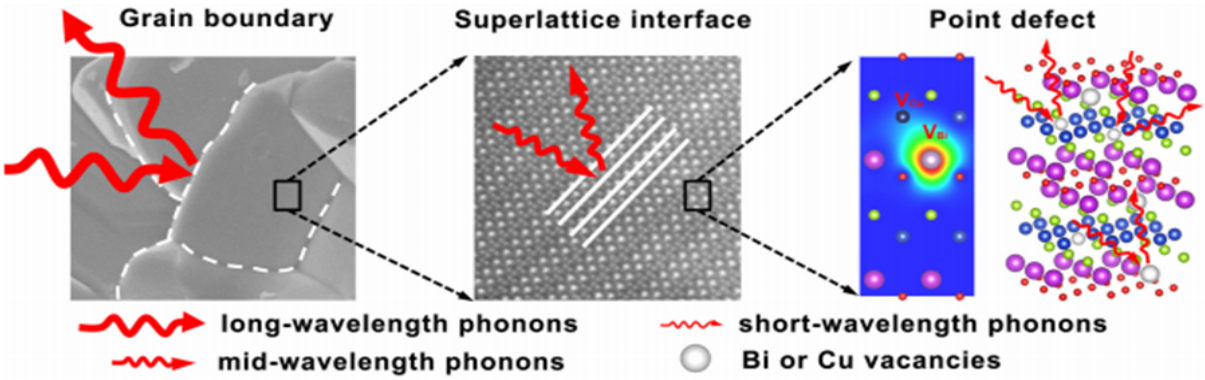

Fig. 10. Representation of various length scale scattering mechanism in BCSO with Bi/Cu vacancies.

5. Bandgap Engineering

Later, the same group reported a slightly higher *ZT* of 1.19 at 873 K. The effect of Sb/Te in BCSO was carried out. Since ball milling is known to induce band convergence leading to higher electrical conductivity as a result of increase in carrier concentration, this method was followed for the synthesis of $Bi_{1-x}Sb_xCu_{1-x}Te_xSeO$ with varying concentration of Sb/Te. It was shown by Li *et al.* that increase in covalency could lead to enhancement in the carrier concentration. Since the electronegativity difference between the $(Bi_2O_2)^{2+}$ and $(Cu_2Se_2)^{2-}$ is large (i.e. (χ_{Bi}~2.02, χ_{o} ~3.44, χ_{Cu} ~1.90, χ_{Se} ~2.55), they replaced the Bi atom with Sb (χ_{Sb} =2.05) which is more electronegative and Se with Te (χ_{Te} =2.1) which is less electronegative. It was seen as the dopant concentration increases, the band gap decreased (from 0.95 to 0.87 eV for undoped and maximum doped (x=0.08) samples respectively) which leads to higher carrier concentration without deteriorating the carrier mobility to much extend (table 2).

Table 2. Variation of optical bandgap of $Bi_{1-x}Sb_xCu_{1-x}Te_xSeO$ with varying dopant concentration

Composition x in $Bi_{1-x}Sb_xCu_{1-x}Te_xSeO$	x=0.00	x=0.02	x=0.04	x=0.08
Optical Band gap (eV)	0.95	0.93	0.90	0.87

Due to the same reason, Seebeck coefficient reduced with doping concentration. However, a promising power factor of ~0.72 $mWm^{-1}K^{-2}$ was reported. As the dopant concentration increased the lattice thermal conductivity was seen to be reducing. On milling for higher duration, i.e 16 h, the lattice thermal conductivity further declined to ~0.46 $Wm^{-1}K^{-1}$, which drove the total thermal conductivity to be the lease for x=0.08. This is due to the electronic contribution to thermal conductivity as a result of high mobility of 5.3 $cm^{-2}V^{-1}s^{-1}$ which is less than the value for BCSO still high enough which lead to increase in total thermal conductivity. Thus, for the Sb/Te doped sample with a maximum milling time of 16 h, they reported a *ZT* of 1.19 at 873 K [46].

6. Spin Seebeck Effect

In 2017, Wen *et al.* were the first group to report the effect of magnetic material doping in BCSO. They carried out dual doping whereby Ba was doped at the Bi site and Ni at the Cu site. Since the magnetic Ni atoms would lead to degeneracies of electronic spin states in real space, it can give rise to further increase in spin entropy which in turn would lead to improvement in Seebeck Coeffienct. A remarkable improvement was observed in the electrical conductivity of

dually doped sample as compared to the pristine sample. High carrier concentration was held responsible for this improvement. However, an optimum concentration of Ni (2%) lead to maximum carrier concentration ($44.4x10^{19}/cm^3$) and electrical conductivity ($6.5x10^3$ S/m) as compared to pristine sample having a carrier concentration of only 0.11 $x10^{19}/cm^3$ and electrical conductivity of ~1.2 $x10^3$ S/m. Also, due to the spin entropy introduced by magnetic Ni atoms, the Seebeck Coeffienct appeared to be as close as the pristine BCSO as seen in figure 11. Maximum Seebeck coefficient of 403 μV/K was exhibited by for x=0.15 in $Bi_{0.875}Ba_{0.125}Cu_{1-x}Ni_xSeO$ which was the highest reported as compared to other reports till then which naturally enhanced the power factor (5 $\mu Wcm^{-1}K^{-2}$). Low thermal conductivity of 0.54 $Wm^{-1}K^{-1}$ at 923 K was reported as a result of suppression of the same by weakening the bonds by dopants. These factors lead to an improved *ZT* of 0.97 from 0.4 at 923 K [47] .

Though BCSO exhibit low thermal conductivity and various strategies have been followed to optimise its electronic performance, it has been seen that the Seebeck coefficient was always compromised. In order to address this issue, Tang *et al.* codoped light element Li and magnetic Mn ions to introduce reduced carrier scattering and increase in Seebeck coefficient by inducing spin entropy respectively. This codoped sample exhibited a jump in carrier mobility ($7.39\ cm^2V^{-1}s^{-1}$) as compared to the pristine BCSO due to the reduction in carrier scattering. A light element like Li holds a better edge than heavy Ba and Sr as they lead to scattering of the charge carriers as well. Since carrier mobility and electrical conductivity is directly related, appreciation in electrical conductivity ($10x10^2$ S/m^{-1}-BCSO to 50 10^2 S/m^{-1} codoped BCSO) was seen. Furthermore, a drastic improvement in Seebeck coefficient was seen for the codoped sample due to the magnetic ion incorporation as compared to previous reports (figure 12).

This improvement in Seebeck coefficient was solely due to the magnetic ion incorporation and band convergence has no role because, the Seebeck coefficient lay above the pisarenko line and that the band calculations also revealed no contribution from hole doping in the improvement of Seebeck coefficient. On further analysis with XPS, it was seen that Mn existed in two oxidation states, i.e +2 and +4 states with a low spin state of ½ and 3/2. These low spin states contribute to the hopping model of spin entropy transfer leading to enhancement in Seebeck coefficient. The spin entropy is given by:

$$S = -\frac{K_B}{e}\left\{\frac{g(Mn^{2+})}{g(Mn)^{4+}}\left[\frac{\rho(Mn^{4+})}{1-\rho(Mn^{4+})}\right]\right\} \quad (5)$$

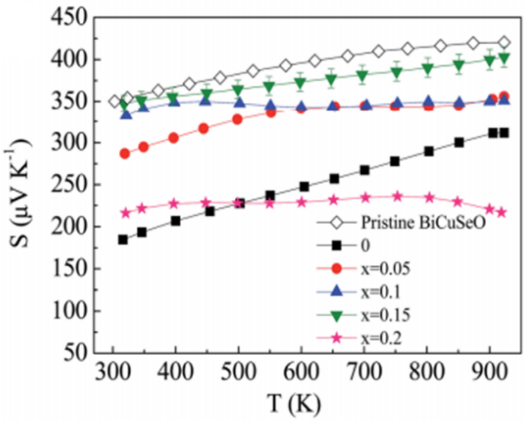

Fig. 11. Temperature dependant variation of Seebeck coefficient with varying dopant concentration.

Where, $g(Mn^{2+})$ and $g(Mn)^{4+}$ are the spin orbital degeneracies for Mn^{2+} and $Mn^{4+}$and $\rho(Mn^{4+})$ is the Mn^{4+} ions concentration. Such an increase in electrical conductivity and Seebeck coefficient lead to an appreciable improvement in PF from 200 $\mu Wm^{-1}K^{-2}$ (BCSO) to 600 $\mu Wm^{-1}K^{-2}$ (Li, Mn codoped BCSO). Very interestingly the total and lattice thermal conductivity was also reported to be the least, lower than pristine BCSO (K_{lat} = 0.6 $Wm^{-1}K^{-1}$) for the codoped samples with x=0.1 in $Bi_{1-x}Li_xCu_{1-x}Mn_xSeO$ (K_{lat} = 0.51 $Wm^{-1}K^{-1}$). These factors contributed to an overall improvement in ZT to 0.9 from ~0.32 at 873K [48].

7. Modulation doping

In 2014, Pei *et al.* reported the highest *ZT* of all times till the date for undoped BCSO exhibiting a *ZT* of 1.4 at 923 K. Such a huge leap from the previously reported *ZT* for pristine sample (0.70 at 773K by Li *et al.* [49]) was mainly because of the improvement of power factor due to modulation doping (MD) strategy. MD strategy have been used in order to maintain an optimum balance between high mobility and low carrier concentration. i.e., pristine BCSO exhibits low carrier concentration but has a descent carrier mobility. However, on doping Ba at the Bi site, the composition exhibits high carrier concentration and low carrier mobility. In order to bridge the features of these 2 compositions, a mix of both the compositions in equal ratios proves to improve the overall thermoelectric performance. Technically fermi energy lays in between the valence and conduction band for pristine BCSO while it lays in the valence band for doped composition. MD essentially induces an imbalance in the fermi level leading to the carrier diffusion from doped phase to pristine phase where carrier mobility is higher owing to the less ionized scattering centres leading to enhanced thermoelectric performance (figure 13). They could improve mobility by 2-fold without deteriorating the carrier concentration. This lead to a high electrical conductivity without and resulted in a very high PF of 10 $\mu Wcm^{-1}K^{-2}$ at 923 K. However, MD had no much influence on the Seebeck coefficient. These factors along with a decrease in κ_{lat} (~0.25 $Wm^{-1}K^{-1}$) lead to *ZT* of 1.4 at 923 K [13].

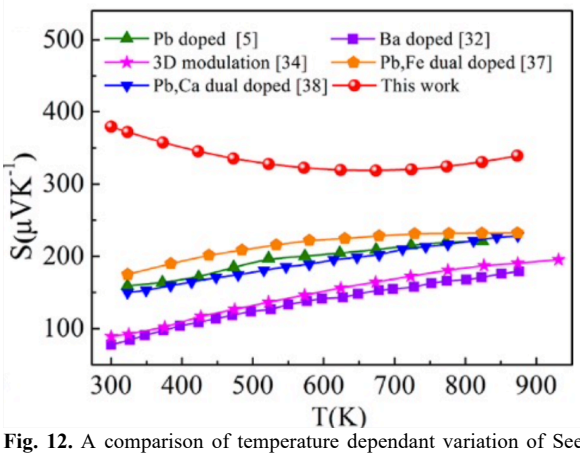

Fig. 12. A comparison of temperature dependant variation of Seebeck coefficient for various reports with that of the Li and Mn codoped BCSO where Mn holds responsible for the introduction of spin entropy leading to enhanced Seebeck coefficient.

In the case of modulation doping, it forms a two-layer configuration. One doped layer and an undoped layer is formed with doped layer giving rise to high concentration of

charge carriers and undoped layer serves as the charge transport channel. It was seen that the electrical conductivity behaviour changed from semi conducting to metallic on doping. The electrical conductivity increased with dopant concentration as dopants lead to increase in carrier concentration. Though the carrier mobility deteriorated with doping which is typical, the change was not marginal.

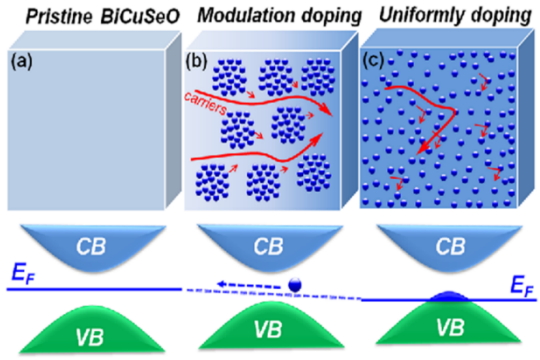

Fig. 13. Three-dimensional schematic showing the band structures and Fermi energy levels for the pristine BiCuSeO, modulation doped and uniformly doped $Bi_{0.875}Ba_{0.125}CuSeO$.

The carrier mobility was reported to be 9.12 $cm^2V^{-1}s^{-1}$ for undoped and 6.56 $cm^2V^{-1}s^{-1}$ for the highest doped sample (x=0.10). High carrier concentration lead to decrease in Seebeck coefficient. While Seebeck coefficient of 381 μVK^{-1} was reported for pure sample, 102 μVK^{-1} was reported for x=0.10. Sine the carrier concentration and mobility were still high for the doped samples, thermal conductivity increased with increasing in dopant concentration (figure 14a). Finally a *ZT* of 1.17 was reported for x=0.10 at 873 K which was higher than the uniformly and heavily doped samples as shown in the (figure 14b) [50].

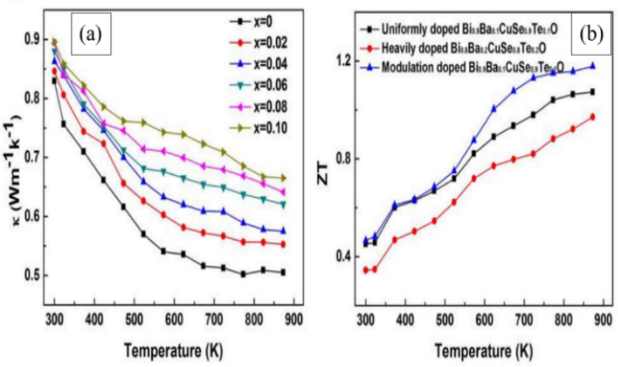

Fig. 14. Temperature dependant variation of thermal conductivity with varying composition of x in $Bi_{1-x}Ba_xCuSe_{1-x}Te_xO$ (a) and the comparison of variation of temperature dependant ZT for uniform, heavily and modulation doped $Bi_{1-x}Ba_xCuSe_{1-x}Te_xO$ where x=0.10 (b)

Since modulation doping had paved way for improvement of thermoelectric parameters, Feng *et al*. in 2019 studied the effect of Lanthanide element (Er) material in the BCSO system. Though La was previously studied, the data suggested that lower electronegativity of 1.10 leads to weak covalent bond between Bi and O as the electronegativity between Bi/La and O becomes larger. Since Er possess higher electronegativity (χ~1.24), high atomic weight and carries only one kind of valency (3+), it makes a suitable dopant for BCSO system. The calculated bandgap suggests that bandgap increased on doping and leads to lower carrier concentration. However, since the carrier mobility increased with doping (9.12- undoped to 39.61 $cm^{-2}V^{-1}s^{-1}$-highly doped), the net electrical conductivity exhibited almost more than 200% increase from 25 S/cm (for pristine) to 133 S/cm (for doped) at 873 K. Seebeck coefficient showed a decrease in trend with doping as charge carrier concentration has inverse relation with Seebeck coefficient. A high-power factor of 0.54 $mWm^{-1}K^{-1}$ was reported for the highly doped sample (x=0.10). The thermal conductivity however increased with doping due to two reasons: the electronic contribution to thermal conductivity increases with doping as n increases; and since Er is a lighter atom than Bi, it results in a quicker sound velocity, high frequency lattice vibration and weak acoustic phonon scattering leading to increase in thermal conductivity and a higher *ZT* of 0.83 was reported for x=0.08. They also reported that out of the simply doped ($Bi_{0.92}Er_{0.08}CuSeO$), heavily doped ($Bi_{0.84}Er_{0.16}CuSeO$) and modulation doped ($Bi_{0.92}Er_{0.08}CuSeO$) samples, modulation doped samples exhibit high electrical conductivity (figure 15a) as it had the characteristic of high carrier concentration from the simply doped and high mobility as of the highly doped sample. Seebeck coefficient however was found to be greater (0.61 $mWm^{-1}K^{-1}$) than the simply doped and highly doped samples due to high electrical conductivity (figure 15b). Due to the different heterostructure that modulation doped samples exhibit, their thermal conductivity was reported to be lower than the other two samples as seen in figure 15d. These factors lead to a much improved *ZT* of 0.99 at 873 K for the modulation doped sample (figure 15f) [51].

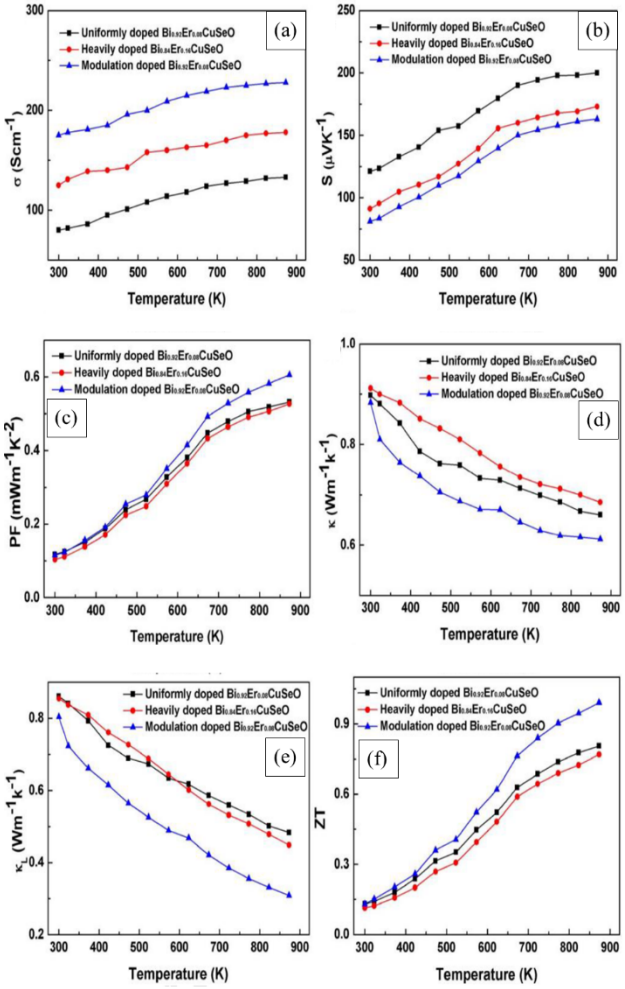

Fig. 15. Temperature dependence of (a) Electrical conductivity (σ), (b) Seebeck coefficient (S), (c) Power factor (PF) (d) Thermal conductivity

(κ), (e) lattice thermal conductivity (κL) and (f) ZT values of the uniformly doped $Bi_{0.92}Er_{0.08}CuSeO$, the heavily doped $Bi_{0.84}Er_{0.16}CuSeO$, and the modulation doped $Bi_{0.92}Er_{0.08}CuSeO$ samples.

Since studies show that Pb has multiple benefits on doping in the BCSO matrix viz. band convergence, increase in carrier concentration, increase in electrical conductivity and high effective mass leading to high Seebeck Coeffienct. Ni has been found to be the best dopant at the Cu site to give raise to high the Seebeck coefficient due to spin entropy effects as reported in 2017 by Wang *et al*.[47], dual doping of these dopants in the BCSO matrix was reported by Feng *et al.* recently in 2019. Earlier reports [13, 50, 51] suggests that modulation doped samples exhibit an improvement in electrical conductivity, power factor and decrease in thermal conductivity. Mechanically alloying was found by the same team to be the best synthesis route for BCSO as it led to ~83% increase in electrical conductivity and high power-factor [41]. So, combining these strategies, Feng *et al.* recently synthesised modulation doped $Bi_{1-x}Pb_xCu_{1-x}Ni_xSeO$ by mechanical alloying method. As expected, the electrical conductivity shot to ~200 S/cm. This was due to leap in carrier concentration. However, the carrier mobility decreased on doping as a result of formation of Pb/Ni defects and nanoprecipitates. Due to the negative correlation between n and S, S decreased with dopant concentration. However, the S was still high enough to lead to a PF of 0.61 $mWm^{-1}K^{-1}$ at 873 K. Though total thermal conductivity increased with doping, lattice thermal conductivity was found to be decreasing with dopant concentration. This is was due to high electrical conductivity due to high carrier concentration. It leads to increase in electronic part of thermal conductivity as they are related. These factors lead to a *ZT* of 1.0 at 873K for 10% Pb/Ni [52].

To understand the effect of modulation doping on this system, Feng *et al.* did a comparative study of uniformly, heavily and modulation doped samples. As on heavy doping, the carrier density would increase, this method exhibited maximum electrical conductivity. Since uniform doping leads to lower carrier concentration than the highly doped sample, as expected, the modulation doped sample exhibited electrical conductivity between the both. The same feature allowed the material to reach a high-power factor of 0.64 $mWm^{-1}K^{-1}$ at 873 K. The thermal conductivity was found to be the least for modulation doped sample mainly due to their unique structure. Since the structure has a combination of pristine and doped sample, the interfaces lead to phonon scattering and lower mean free path for the phonons. Hence the thermal conductivity declines. Thus, an improved *ZT* of 1.08 at 873 K was reported for the modulation doped sample [52]. A comparison of Pb doped BCSO [22] and Ni doped BCSO [47] with that of Pb/Ni co-doped BCSO and effect of modulation doping [52]. It can be clearly seen that the thermoelectric parameters have been improved on each stage leading to maximum *ZT* for the codoped sample that is modulation doped.

In summary, table 4 gives thermoelectric parameters of BCSO based compounds that exhibit promising thermoelectric figure of merit.

Table 3. A comparison of electrical conductivity, Seebeck coefficient, power factor, thermal conductivity and ZT for pristine BCSO, Pb doped, Ni doped, Pb/Ni codoped and Pb/Ni modulation doped compositions.

Parameters	Element						
	Pb		Ni		Pb/Ni		
					Normally doped		Modulation doped
	Pristine	Doped	Pristine	Doped	Pristine	Doped	
Electrical Conductivity (σ) S/cm	~50	~220	~1 x 10^3	~3.5	~30	~200	~220
Seebeck coefficient (S) μVK^{-1}	~380	~221	~400	~375	~320	~160	~150
Power factor ($S^2\sigma$) $mWm^{-1}K^{-1}$	~1	~7.3	~2	~5.5	~0.28	~0.61	~0.64
Thermal conductivity (κ) $Wm^{-1}K^{-1}$	~0.4	~0.6	~0.6	~0.54	~0.5	~0.6	~0.58
ZT	~0.32	~1.14	~0.38	~0.97	~0.45	~1.06	~1.08

Table 4. A summary of all the thermoelectric parameters at room temperature and temperature corresponding to highest ZT is given in the table.

Sl. No	Composition	Resistivity/Conductivity		α(μV/K)		K (W/m-K)		PF *(W/cm-K^2)		ZT		Ref.
		RT		RT		RT		RT			T	
1	$Bi_{0.925}Sr_{0.075}CuSeO$	2x10^4 S/m	1 x10^4 S/m	120	225	1.05	0.65	-	500 μ	0.76	873 K	[53]
2	$BiCu_{0.975}SeO$	0.2x10^4 log S/cm	0.5 x10^4 log S/cm	165	265	0.8	0.5	0.6 μ	4.3 μ	0.8	650 K	[54]
3	$Bi_{0.875}Ba_{0.125}CuSeO$	450 (S/cm)	190 S/cm	69	167	0.75	0.48	3 μ	6.2 μ	1.1	923 K	[55]

4	$Bi_{0.925}Ca_{0.075}CuSeO$	300 S/cm	110 S/cm	150	220	0.89	0.65	710 μ	610 μ	0.8	773 K	[56]
5	$Bi_{0.925}Ca_{0.075}CuSeO$	3 x 10^{-2} (S/cm)	1 x 10^{-2} (S/cm)	155	240	1.05	0.49	1.2 μ	4.8 μ	0.9	923K	[57]
6	$Bi_{0.92}Pb_{0.08}CuSeO$	560	180	80	170	0.86	0.55	550 μ	555 μ	0.95	873 K	[58]
7	$Bi_{0.875}Ba_{0.125}CuSeO$	710 (S/cm)	210 (S/cm)	76	190	0.9	0.58	5 μ	8.1 μ	1.4	923 K	[59]
8	$Bi_{0.985}Na_{0.015}CuSeO$	125	50	265	290	0.81	0.5	6.5 μ	4.5 μ	0.91	923 K	[60]
9	Modulation doped $Bi_{0.875}Ba_{0.125}CuSeO$	650 (S/cm)	290 S/cm	80	200	1.1	0.69	4.8 μ	10 μ	1.4	923 K	[61]
10	$BiCu_{0.99}Zn_{0.1}SeO$	1900	4500	375	280	1	0.39	2.55 μ	4.21 μ	0.90	873 K	[62]
11	$Bi_{0.94}Pb_{0.06}CuSeO$	545(S/cm)	200(S/cm)	125	190	1.12	0.78	8.1 μ	7.9 μ	0.91	873 K	[63]
12	$Bi_{0.92}Na_{0.08}CuSeO$	60	100	175	250	1	0.5	510 μ	460 μ	0.97	873 K	[64]
13	$Bi_{1-0.05}Cd_{0.05}CuSeO$	170 (S/cm)	73 (S/cm)	180	245	0.81	0.40	593 μ	450 μ	0.98	923 K	[65]
14	$Bi_{0.88}Ca_{0.06}Pb_{0.06}CuSeO$	$4.6x10^2$ (S/cm)	$1.6\ x10^2$ (S/cm)	148	230	0.79	0.52	$1x10^{-3}$	$8.4x10^{-4}$	1.5	873 K	[66]
15	$Bi_{0.94}Pb_{0.06}CuSeO$	500(S/cm)	160(S/cm)	130	220	1.04	0.58	-	-	1.2	923 K	[67]
16	$Bi_{0.96}Pb_{0.04}CuSe_{0.075}Te_{0.925}O$	250(S/cm)	100(S/cm)	170	240	0.3	0.7	7.5 μ	6 μ	1.2	800 K	[68]
17	$Bi_{0.875}Ba_{0.125}Cu_{0.85}Ni_{0.15}SeO$	24 S/cm)	35 S/cm)	350	400	1.11	0.53	2.8 μ	5.6 μ	0.97	923 K	[69]
18	BiCuSeO	0.010 m Ω-cm	0.025 m Ω-cm	88	160	0.93	0.71	0.71 m	1.01m	1.09	773 K	[70]
19	$Bi_{0.88}Mg_{0.06}Pb_{0.06}CuSeO$	900(S/cm)	260(S/cm)	100	180	1.08	0.7	8.8 μ	11 μ	1.19	750 K	[71]
20	$Bi_{0.88}Ba_{0.06}Pb_{0.06}CuSeO$	345 (S/cm)	170 (S/cm)	120	195	0.88	0.64	0.43	0.66m	1.01	873 K	[72]
21	$Bi_{0.84}Ca_{0.08}Pb_{0.08}CuSeO$	440(S/cm)	200(S/cm)	90	190	0.88	0.66	0.38m	0.77m	1.15	873 K	[73]
22	$Bi_{0.92}Sb_{0.08}CuSe_{0.92}Te_{0.08}O$	530 (S/cm)	280 S/cm)	70	160	0.85	0.6	0.22	0.72	1.19	873 K	[74]
23	Modulation doped $Bi_{0.9}Ba_{0.10}CuSe_{0.90}Te_{0.10}O$	450 S/cm)	255 S/cm)	115	190	1.18	0.83	0.53m	1m	1.17	873 K	[75]
24	Modulation doped $Bi_{0.92}Er_{0.08}CuSeO$	175	225	80	165	0.89	0.62	0.11m	0.6m	0.99	873 K	[76]
25	Modulation doped $Bi_{0.90}Pb_{0.10}Cu_{0.90}Ni_{0.10}SeO$	340	220	85	170	0.88	0.58	0.28m	0.64m	1.08	873 K	[52]
26	$Bi_{0.86}Pb_{0.14}CuSeO$	-	-	-	93	-	-	9.5 μ	11.4 μ	1.3	873 K	[35]
27	80% fine + 20% course powder of $Bi_{0.94}In_{0.06}CuSeO$	123S/cm	200S/cm	100	172	0.7	0.48	0.12m	0.58	1.08	873K	[77]

8. Conclusion

In this review, we have identified various strategies by which BiCuSeO can be tuned for better performance. The various strategies discussed are single carrier doping, co-doping technique, defect engineering, bandgap engineering, modulation doping and spin Seebeck effect. One of the key highlights of BCSO is the substantially low thermal conductivity. Hence, a lot of reports highlight the improvement of electrical conductivity by various doping strategies and texturization. While all the techniques have led to improvement in thermoelectric parameters, the most promising method to tune BCSO for better performance have been found to be modulation doping. For improvement in the thermoelectric parameters, the authors feel the need to combine two techniques. i.e., modulation doping has to be followed by texturization. Such a study might have the potential to push ZT further as, anisotropy driven features are absent in the just modulation doped material. Although the past decade had been very fruitful for BCSO research and has been able to progress in ZT without the presence of Pb, systematic studies on the effect of each texturization techniques such as hot pressing, hot forging and spark plasma sintering can be carried out on the modulation doped compositions to realise insights into its anisotropic transport properties. Lastly, since BCSO is a p-type compound, a suitable n-type counterpart has to be developed for practical applications along with suitable contacts.

References

1. Seebeck, T.J., Ueber die magnetische Polarisation der Metalle und Erze durch Temperaturdifferenz. Annalen der Physik, 1826. **82**(3): p. 253-286.
2. Vedernikov, M. and E. Iordanishvili. AF Ioffe and origin of modern semiconductor thermoelectric energy conversion. in Seventeenth International Conference on Thermoelectrics. Proceedings ICT98 (Cat. No. 98TH8365). 1998. IEEE.
3. Taroni, P.J., et al., Thermoelectric materials: A brief historical survey from metal junctions and inorganic semiconductors to organic polymers. Israel Journal of Chemistry, 2014. **54**(5-6): p. 534-552.
4. Rowe, D.M., CRC handbook of thermoelectrics. 1995: CRC press.
5. Snyder, G.J., E.S.J.M.f.s.e.a.c.o.p.-r.r. Toberer, and r.a.f.N.P. Group, Complex thermoelectric materials. 2011: p. 101-110.
6. Toberer, E., Complex thermoelectric materials. Nat Mater, 2008. **7**(2): p. 105114Son.
7. Zhang, X. and L.-D. Zhao, Thermoelectric materials: Energy conversion between heat and electricity. Journal of Materiomics, 2015. **1**(2): p. 92-105.
8. Han, L., et al., Effects of morphology on the thermoelectric properties of Al-doped ZnO. RSC Advances, 2014. **4**(24): p. 12353-12361.
9. Combe, E., et al., Synthesis of In 2− x Ge x O 3 nanopowders for thermoelectric applications. Journal of Materials Research, 2012. **27**(2): p. 500-505.
10. Ekren, D., et al., Enhancing the thermoelectric power factor of Sr 0.9 Nd 0.1 TiO 3 through control of the nanostructure and microstructure. Journal of Materials Chemistry A, 2018. **6**(48): p. 24928-24939.
11. Funahashi, R., et al., An oxide single crystal with high thermoelectric performance in air. Japanese Journal of Applied Physics, 2000. **39**(11B): p. L1127.
12. Yakabe, H., et al. Thermoelectric properties of transition-metal oxide NaCo/sub 2/O/sub 4/system. in XVI ICT'97. Proceedings ICT'97. 16th International Conference on Thermoelectrics (Cat. No. 97TH8291). 1997. IEEE.
13. Pei, Y.-L., et al., High thermoelectric performance realized in a BiCuSeO system by improving carrier mobility through 3D modulation doping. Journal of the American Chemical Society, 2014. **136**(39): p. 13902-13908.
14. Zhao, L.-D., et al., BiCuSeO oxyselenides: new promising thermoelectric materials. Energy & Environmental Science, 2014. **7**(9): p. 2900-2924.
15. Barreteau, C.l., et al., Structural and electronic transport properties in Sr-doped BiCuSeO. Chemistry of Materials, 2012. **24**(16): p. 3168-3178.
16. Zhao, L., et al., Bi 1− x Sr x CuSeO oxyselenides as promising thermoelectric materials. Applied Physics Letters, 2010. **97**(9): p. 092118.
17. Li, J., et al., A high thermoelectric figure of merit ZT> 1 in Ba heavily doped BiCuSeO oxyselenides. Energy & Environmental Science, 2012. **5**(9): p. 8543-8547.
18. Li, F., et al., Enhanced thermoelectric performance of Ca-doped BiCuSeO in a wide temperature range. Journal of Materials Chemistry A, 2013. **1**(38): p. 11942-11949.
19. Pei, Y.-L., et al., High thermoelectric performance of oxyselenides: intrinsically low thermal conductivity of Ca-doped BiCuSeO. NPG Asia Materials, 2013. **5**(5): p. e47.
20. Pan, L., et al., Influence of Pb doping on the electrical transport properties of BiCuSeO. Applied Physics Letters, 2013. **102**(2): p. 023902.
21. Liu, Y.c., et al., Thermoelectric Properties of Pb-Doped BiCuSeO Ceramics. Journal of the American Ceramic Society, 2013. **96**(9): p. 2710-2713.
22. Lan, J.L., et al., Enhanced thermoelectric properties of Pb-doped BiCuSeO ceramics. Advanced Materials, 2013. **25**(36): p. 5086-5090.
23. Sui, J., et al., Texturation boosts the thermoelectric performance of BiCuSeO oxyselenides. Energy & Environmental Science, 2013. **6**(10): p. 2916-2920.
24. Li, J., et al., The roles of Na doping in BiCuSeO oxyselenides as a thermoelectric material. Journal of Materials Chemistry A, 2014. **2**(14): p. 4903-4906.
25. Ren, G.K., et al., Enhanced thermoelectric performance of Zn-doped oxyselenides: BiCu1− xZnxSeO. physica status solidi (a), 2014. **211**(11): p. 2616-2620.
26. Ren, G.-K., et al., Enhanced thermoelectric properties in Pb-doped BiCuSeO oxyselenides prepared by ultrafast synthesis. RSC Advances, 2015. **5**(85): p. 69878-69885.
27. Zhang, M., et al., Multi-role of sodium doping in BiCuSeO on high thermoelectric performance. Journal of Electronic Materials, 2015. **44**(8): p. 2849-2855.
28. Farooq, M., et al., Cd-doping a facile approach for better thermoelectric transport properties of BiCuSeO oxyselenides. RSC Advances, 2016. **6**(40): p. 33789-33797.
29. Yang, D., et al., Manipulating the Combustion Wave during Self-Propagating Synthesis for High Thermoelectric Performance of Layered Oxychalcogenide Bi1–x Pb x CuSeO. Chemistry of Materials, 2016. **28**(13): p. 4628-4640.
30. Zhu, H., et al., Effects of high pressure sintering on the microstructure and thermoelectric properties of BiCuSeO. High Pressure Research, 2017. **37**(1): p. 36-45.
31. Zhu, H., et al., High pressure synthesis, structure and thermoelectric properties of BiCuChO (Ch= S, Se, Te). Journal of the European Ceramic Society, 2017. **37**(4): p. 1541-1546.
32. Farooq, M.U., et al., Improved thermoelectric performance of BiCuSeO by Ag substitution at Cu site. Journal of Alloys and Compounds, 2017. **691**: p. 572-577.
33. Sun, Y., et al., Enhanced thermoelectric properties and electronic structures of p-type BiCu1− xAgxSeO ceramics. Ceramics International, 2017. **43**(8): p. 6117-6123.
34. Das, S., et al., Thermoelectric properties of Sn doped BiCuSeO. Applied Surface Science, 2017. **418**: p. 238-245.
35. Ren, G.-K., et al., Complex electronic structure and compositing effect in high performance thermoelectric BiCuSeO. 2019. **10**(1): p. 1-9.
36. Feng, B., et al., Enhancement of the Thermoelectric Properties of BiCuSeO via In Doping and Powder Size Controlling. Journal of Electronic Materials, 2020. **49**(1): p. 611-620.
37. Liu, Y., et al., Synergistically optimizing electrical and thermal transport properties of BiCuSeO via a dual-doping approach. Advanced Energy Materials, 2016. **6**(9): p. 1502423.
38. Ren, G.-K., et al., Enhancing thermoelectric performance in hierarchically structured BiCuSeO by increasing bond covalency and weakening carrier–phonon coupling. Energy & Environmental Science, 2017. **10**(7): p. 1590-1599.
39. Sun, Y., et al., Co-doping for significantly improved thermoelectric figure of merit in p-type Bi1-2xMgxPbxCuSeO oxyselenides. Ceramics International, 2017. **43**(18): p. 17186-17193.
40. Feng, B., et al., Effect of Ba and Pb dual doping on the thermoelectric properties of BiCuSeO ceramics. Materials Letters, 2018. **217**: p. 189-193.
41. Feng, B., et al., Effect of synthesis processes on the thermoelectric properties of BiCuSeO oxyselenides. Journal of Alloys and Compounds, 2018. **754**: p. 131-138.
42. Liu, Y.-c., et al., Influence of Ag doping on thermoelectric properties of BiCuSeO. Journal of the European Ceramic Society, 2015. **35**(2): p. 845-849.
43. Li, F., et al., Synergetic Tuning of the Electrical and Thermal Transport Properties via Pb/Ag Dual Doping in BiCuSeO. ACS Applied Materials & Interfaces, 2019. **11**(49): p. 45737-45745.
44. Liu, Y., et al., Remarkable enhancement in thermoelectric performance of BiCuSeO by Cu deficiencies. Journal of the American Chemical Society, 2011. **133**(50): p. 20112-20115.
45. Li, Z., et al., Dual vacancies: an effective strategy realizing synergistic optimization of thermoelectric property in BiCuSeO. Journal of the American Chemical Society, 2015. **137**(20): p. 6587-6593.
46. Feng, B., et al., Enhancing thermoelectric and mechanical performances in BiCuSeO by increasing bond covalency and nanostructuring. Journal of Solid State Chemistry, 2018. **265**: p. 306-313.
47. Wen, Q., et al., Enhanced thermoelectric performance of BiCuSeO by increasing Seebeck coefficient through magnetic ion incorporation. Journal of Materials Chemistry A, 2017. **5**(26): p. 13392-13399.
48. Tang, J., et al., Light element doping and introducing spin entropy: an effective strategy for enhancement of thermoelectric properties in BiCuSeO. 2019. **11**(17): p. 15543-15551.
49. Li, F., et al., Polycrystalline BiCuSeO oxide as a potential thermoelectric material. 2012. **5**(5): p. 7188-7195.

50. Feng, B., et al., Enhanced thermoelectric performance in BiCuSeO oxyselenides via Ba/Te dual-site substitution and 3D modulation doping. Journal of Solid State Chemistry, 2018. **266**: p. 297-303.
51. Feng, B., et al., Enhanced thermoelectric performances in BiCuSeO oxyselenides via Er and 3D modulation doping. Ceramics International, 2019. **45**(4): p. 4493-4498.
52. Feng, B., et al., Enhanced thermoelectric properties in BiCuSeO ceramics by Pb/Ni dual doping and 3D modulation doping. 2019. **271**: p. 1-7.
53. Zhao, L., et al., Bi 1− x Sr x CuSeO oxyselenides as promising thermoelectric materials. 2010. **97**(9): p. 092118.
54. Liu, Y., et al., Remarkable enhancement in thermoelectric performance of BiCuSeO by Cu deficiencies. 2011. **133**(50): p. 20112-20115.
55. Li, J., et al., A high thermoelectric figure of merit ZT> 1 in Ba heavily doped BiCuSeO oxyselenides. 2012. **5**(9): p. 8543-8547.
56. Li, F., T. Wei, and F.J.J.M.C.A. Kang, L., J. Enhanced thermoelectric performance of Ca-doped BiCuSeO in a wide temperature range. 2013. **1**: p. 11942-11949.
57. Pei, Y., et al., High thermoelectric performance of oxyselenides: Intrinsically low thermal conductivity of Ca-doped BiCuSeO, NPG Asia Mater. 5 (2013) e47. 2013.
58. Liu, Y.c., et al., Thermoelectric Properties of Pb-Doped BiCuSeO Ceramics. 2013. **96**(9): p. 2710-2713.
59. Sui, J., et al., Texturation boosts the thermoelectric performance of BiCuSeO oxyselenides. 2013. **6**(10): p. 2916-2920.
60. Li, J., et al., The roles of Na doping in BiCuSeO oxyselenides as a thermoelectric material. 2014. **2**(14): p. 4903-4906.
61. Pei, Y.-L., et al., High thermoelectric performance realized in a BiCuSeO system by improving carrier mobility through 3D modulation doping. 2014. **136**(39): p. 13902-13908.
62. Ren, G.K., et al., Enhanced thermoelectric performance of Zn-doped oxyselenides: BiCu1− xZnxSeO. 2014. **211**(11): p. 2616-2620.
63. Ren, G.-K., et al., Enhanced thermoelectric properties in Pb-doped BiCuSeO oxyselenides prepared by ultrafast synthesis. 2015. **5**(85): p. 69878-69885.
64. Zhang, M., et al., Multi-role of sodium doping in BiCuSeO on high thermoelectric performance. 2015. **44**(8): p. 2849-2855.
65. Farooq, M., et al., Cd-doping a facile approach for better thermoelectric transport properties of BiCuSeO oxyselenides. 2016. **6**(40): p. 33789-33797.
66. Liu, Y., et al., Synergistically optimizing electrical and thermal transport properties of BiCuSeO via a dual-doping approach. 2016. **6**(9): p. 1502423.
67. Yang, D., et al., Manipulating the Combustion Wave during Self-Propagating Synthesis for High Thermoelectric Performance of Layered Oxychalcogenide Bi1–x Pb x CuSeO. 2016. **28**(13): p. 4628-4640.
68. Ren, G.-K., et al., Enhancing thermoelectric performance in hierarchically structured BiCuSeO by increasing bond covalency and weakening carrier–phonon coupling. 2017. **10**(7): p. 1590-1599.
69. Wen, Q., et al., Enhanced thermoelectric performance of BiCuSeO by increasing Seebeck coefficient through magnetic ion incorporation. 2017. **5**(26): p. 13392-13399.
70. Das, S., et al., Thermoelectric properties of Sn doped BiCuSeO. 2017. **418**: p. 238-245.
71. Sun, Y., et al., Co-doping for significantly improved thermoelectric figure of merit in p-type Bi1-2xMgxPbxCuSeO oxyselenides. 2017. **43**(18): p. 17186-17193.
72. Feng, B., et al., Effect of Ba and Pb dual doping on the thermoelectric properties of BiCuSeO ceramics. 2018. **217**: p. 189-193.
73. Feng, B., et al., Effect of synthesis processes on the thermoelectric properties of BiCuSeO oxyselenides. 2018. **754**: p. 131-138.
74. Feng, B., et al., Enhancing thermoelectric and mechanical performances in BiCuSeO by increasing bond covalency and nanostructuring. 2018. **265**: p. 306-313.
75. Feng, B., et al., Enhanced thermoelectric performance in BiCuSeO oxyselenides via Ba/Te dual-site substitution and 3D modulation doping. 2018. **266**: p. 297-303.
76. Feng, B., et al., Enhanced thermoelectric performances in BiCuSeO oxyselenides via Er and 3D modulation doping. 2019. **45**(4): p. 4493-4498.
77. Feng, B., et al., Enhancement of the Thermoelectric Properties of BiCuSeO via In Doping and Powder Size Controlling. 2020. **49**(1): p. 611-620.